

CPPM: Chi-squared Progressive Photon Mapping

Supplementary Material

ZEHUI LIN, SHENG LI*, XINLU ZENG, and CONGYI ZHANG, Dept. of Computer Science and Technology, Peking University

JINZHU JIA, Dept. of Biostatistics and Center for Statistical Science, Peking University

GUOPING WANG, Dept. of Computer Science and Technology, Peking University

DINESH MANOCHA, University of Maryland at College Park

CCS Concepts: • Computing methodologies → Rendering.

Additional Key Words and Phrases: progressive photon mapping, chi-squared test, probability density function, radiance estimate, mean squared error

1 CONVERGENCE COMPARISONS OF SPPM, APPM AND CPPM

We show the variation of MSE over iterations for SPPM, APPM, and CPPM for all benchmarks in log-log plot in Fig. 1. The initial bandwidths for all the methods are determined by $k_{NN} = 10$ using k-NN search [Hachisuka and Jensen 2009]. The optimal setting $\alpha = 2/3$ is used for SPPM [Kaplyanyan and Dachsbacher 2013]. We use $n_a = 2$, $n_s = 6$, $k = 0.8$ and $\beta = 1.2$ for CPPM unless otherwise stated. The same number of photons 2^{16} per iteration is used for all the methods. Our method (CPPM) exhibits the best performance.

2 DIFFERENT β CAN RESULT IN DIFFERENT CONVERGENCE SPEED IN OUR METHOD.

We demonstrate the plots of MSE over iterations on the Diamond, Sibenik, and Torus scenes using different β for our method (CPPM), ranging from 1.0 to 1.5 in Fig. 2. The slope of different β is scene-dependent, which implies that β can affect the convergence of our method.

3 PSEUDOCODE OF CPPM

Algorithm 1 shows the pseudocode of CPPM.

4 LIGHT LEAK PROBLEM

Light leak [Jensen 2004] is a special problem that may occur in some scenes when rendered using photon mapping method. This is caused by wrongly collecting the photons located behind another object. These photons should be blocked although they are actually located in the bandwidth. In general, the larger the bandwidth for collection, the more serious the light leak problem. In Fig. 3, we show the light

*corresponding author: lisheng@pku.edu.cn

Project URL: bactlink.github.io/CPPM

Permission to make digital or hard copies of all or part of this work for personal or classroom use is granted without fee provided that copies are not made or distributed for profit or commercial advantage and that copies bear this notice and the full citation on the first page. Copyrights for components of this work owned by others than ACM must be honored. Abstracting with credit is permitted. To copy otherwise, or republish, to post on servers or to redistribute to lists, requires prior specific permission and/or a fee. Request permissions from permissions@acm.org.

© 2020 Association for Computing Machinery.

0730-0301/2020/12-ART1 \$15.00

<https://doi.org/10.1145/3414685.3417822>

Algorithm 1: CPPM

```
for each pixel do
     $R_1 \leftarrow$  Initialize bandwidth by  $k_{NN}$ ;
     $B_1 \leftarrow k_{NN}$ ;
    Photon Counter  $\leftarrow 0$ ;
     $\forall a, \forall s, O_{a,s} \leftarrow 0$ ;
end
for iteration  $i \leftarrow 1$  to  $\infty$  do
    for each pixel do
        | Ray tracing from eye and obtain the hit point  $\vec{x}_i$ ;
    end
    Generate photon map;
    for each pixel do
        | Update pixel measurement estimate;
        | Map the photons to the unified domain  $\Omega_{R_i}$  and
        | align;
        |  $\forall a, \forall s, O_{a,s} +=$  number of photons in the  $s$ -th sector
        | of the  $a$ -th annulus;
        | Photon Counter  $+=$  number of collected photons;
        if  $\text{Photon Counter} \geq B_i$  and
            the chi-squared test rejects the null hypothesis then
            | Obtain  $R_{i+1}$ ;
            | Photon Counter  $\leftarrow 0$ ;
            |  $\forall a, \forall s, O_{a,s} \leftarrow 0$ ;
            |  $B_{i+1} \leftarrow \beta B_i$ ;
            | Partition the new unified domain  $\Omega_{R_{i+1}}$ ;
        else
            |  $R_{i+1} \leftarrow R_i$ ;
            |  $B_{i+1} \leftarrow B_i$ ;
        end
    end
end
```

leak phenomenon occurs at the corner of the Dining Room by SPPM, APPM and CPPM, respectively. None of these methods employ special treatment to handle this problem. However, APPM shows the most obvious light leak problem in the dark region. This is because the bias and variance estimated by APPM are not very accurate, and the bias is underestimated. Therefore, a larger bandwidth is used to reduce variance meanwhile the light leak being introduced. Through careful observation, we can see that the light leak in CPPM is slightly

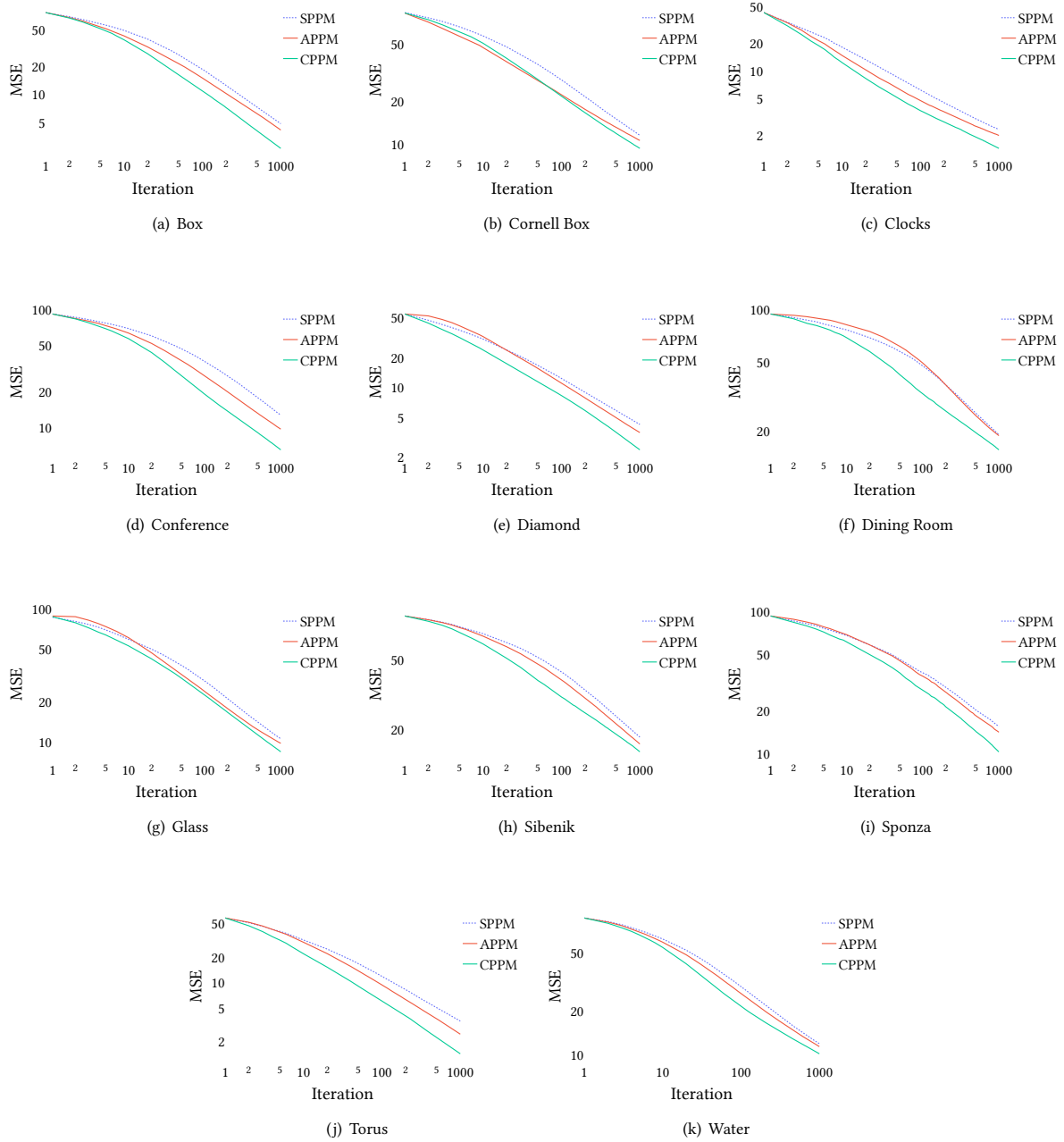


Fig. 1. MSE over iterations for all benchmarks in log-log plot, CPPM exhibits the best performance in all scenes.

less than SPPM (but not obvious). The light leak phenomenon is inevitable without special processing.

5 OTHER SUFFICIENT CONDITIONS FOR UNBIASED ESTIMATION

In section 4 of the main body, we show that if the average photon density function (APDF) is a constant function, the estimation is unbiased under our assumptions. In addition to constant functions, generalized odd functions (GOF, odd functions with constant

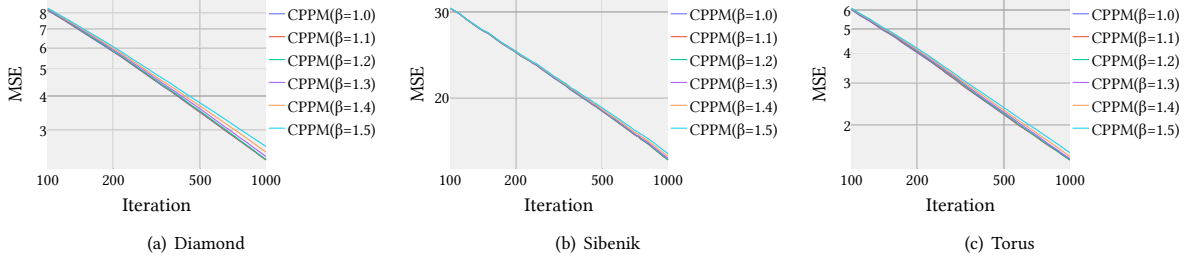
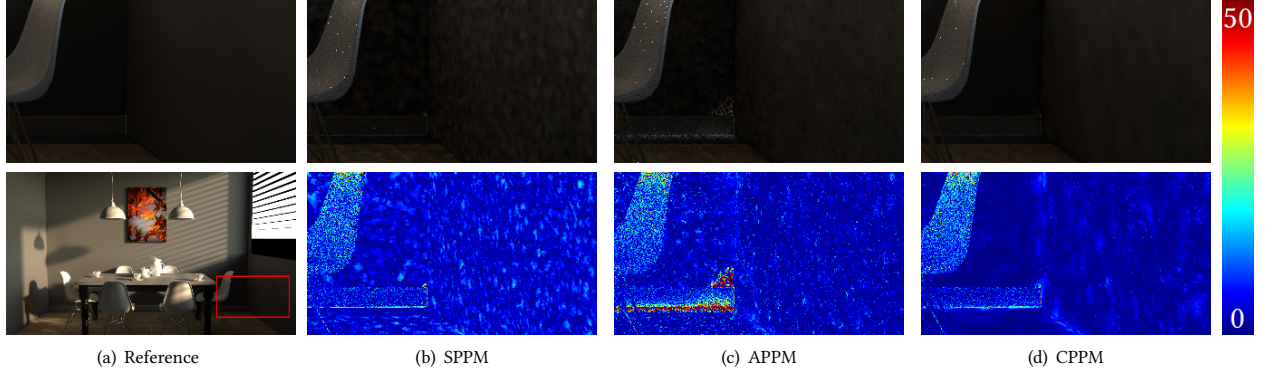

 Fig. 2. Different β on Diamond


Fig. 3. Close-up images of the Dining scene. The heat map visualizes the absolute difference w.r.t. the reference image; the blue to red color scale corresponds to a small to large error range. CPPM exhibit the slightest light leak phenomenon compared to other methods.

offset) can also be used as the sufficient conditions for unbiased estimation under our assumptions. We will give a proof as well as implementation details in this section.

5.1 Theoretical Proof

In the main body, we have shown that the pixel measurement estimation is unbiased if and only if

$$I = E \left[\int_{\Omega_R} k_R(\vec{x}') \bar{p}(\vec{x}') d\vec{x}' \right] E \left[\tilde{\Psi} \right] \quad (1)$$

under our assumptions.

Formally, the APDF is a generalized odd function implies

$$\forall \vec{x}' \in \Omega_R, (\bar{p}(\vec{x}') + \bar{p}(-\vec{x}')) \equiv C \equiv 2E[\bar{p}], \quad (2)$$

where C is a constant.

Doubling both sides of Eq. (1), since the kernel function is isotropic and circular, it becomes

$$\begin{aligned} 2I &= E \left[2 \int_{\Omega_R} k_R(\vec{x}') \bar{p}(\vec{x}') d\vec{x}' \right] E \left[\tilde{\Psi} \right] \\ 2I &= E \left[\int_{\Omega_R} k_R(\vec{x}') (\bar{p}(\vec{x}') + \bar{p}(-\vec{x}')) d\vec{x}' \right] E \left[\tilde{\Psi} \right]. \end{aligned} \quad (3)$$

Substituting $(\bar{p}(\vec{x}') + \bar{p}(-\vec{x}'))$ using Eq. (2), Eq. (3) becomes

$$I = E \left[\int_{\Omega_R} k_R(\vec{x}') d\vec{x}' \right] E [\bar{p}] E \left[\tilde{\Psi} \right], \quad (4)$$

where the first term on the right side equals one.

Note that since the expected value of a radiance estimate with an infinitely small kernel bandwidth corresponds to the exact radiance [Knaus and Zwicker 2011], we can express I as

$$I = E \left[\tilde{\Psi} \right] E \left[\delta(\vec{x}') \right] = E \left[\tilde{\Psi} \right] E \left[\bar{p}(\vec{0}) \right], \quad (5)$$

where δ is the Dirac delta function. Eq. (5) explains that Eq. (4) is true. Therefore, the pixel measurement estimation is also unbiased when the APDF is a generalized odd function under our assumptions.

Generalize odd functions cover a large range of functions, such as linear functions whose first derivative is 0. Any subset of generalize odd functions can also be used as a sufficient condition for unbiased estimation.

5.2 Implementation

5.2.1 Generalized Odd Function. The average function of any generalized odd function and its centrally symmetric function is a constant function. Therefore, we only have to test whether this average function is a constant function. To this end, each photon has a 50%

probability to be converted from $\vec{p}'_{i,j}$ to its opposite position $-\vec{p}'_{i,j}$. After such random conversion of photons, we obtain the samples of the average function described above. Then, the test process is the same as that of constant function described in the main body.

5.2.2 Linear Function. 2D Linear density function can be represented as

$$f(\vec{x}) = (k_1, k_2) \cdot \vec{x} + c, \text{ s.t. } \forall \vec{x} \in \bar{\Omega}, f(\vec{x}) \geq 0, \quad (6)$$

$$\int_{\bar{\Omega}} f(\vec{x}) d\vec{x} = 1,$$

where k_1, k_2 and c are coefficients of the linear function. Before performing the chi-squared test, we have to estimate these three coefficients to make the model best fit the observations first. Then we can integrate the function over each sector to obtain $p_{a,s}$ in Eq. (12) in the main body. It is not easy to obtain the coefficients by minimum chi-squared estimation or maximum likelihood estimation, so we use least square estimation instead.

Since $f(\vec{x})$ is subject to GOF and Ω_R is a disc, we can obtain the value of c from the integral constraint:

$$\int_{\Omega_R} f(\vec{x}) d\vec{x} = c\pi R^2 = 1 \quad (7)$$

$$\Rightarrow c = \frac{1}{\pi R^2}.$$

Coefficient k_1 and k_2 are obtained by least square estimation as

$$k_1, k_2 = \arg \min_{k_1, k_2} \sum_{a=1}^{n_a} \sum_{s=1}^{n_s} (O_{a,s} - Mp_{a,s})^2, \quad (8)$$

where n_a and n_s are partition parameters, M is the total number of photons collected in Ω_R , $O_{a,s}$ is the number of photons collected in the s -th sector of the a -th annulus, and $p_{a,s}$ is the expected probability of the s -th sector of the a -th annulus.

Under the null hypothesis of linear function, $p_{a,s}$ can be obtained by integrating f over the corresponding sector $\Omega_{a,s}$ as:

$$p_{a,s} = \int_{\Omega_{a,s}} f(\vec{x}) d\vec{x}$$

$$= \int_{R\sqrt{\frac{a-1}{n_a}}}^{R\sqrt{\frac{a}{n_a}}} \int_{\frac{2(s-1)\pi}{n_s}}^{\frac{2s\pi}{n_s}} (k_1 r^2 \cos(\theta) + k_2 r^2 \sin(\theta) + cr) dr d\theta$$

$$= \frac{2}{3} \left(a^{\frac{3}{2}} - (a-1)^{\frac{3}{2}} \right) \cos \left(\frac{(2s-1)\pi}{n_s} \right) \sin \left(\frac{\pi}{n_s} \right) n_a^{\frac{2}{3}} R^3 k_1 \quad (9)$$

$$+ \frac{2}{3} \left(a^{\frac{3}{2}} - (a-1)^{\frac{3}{2}} \right) \sin \left(\frac{(2s-1)\pi}{n_s} \right) \sin \left(\frac{\pi}{n_s} \right) n_a^{\frac{2}{3}} R^3 k_2$$

$$+ \frac{1}{n_a n_s}.$$

Then we solve Eq. (LSE-equation) by finding its critical point and get the initial value of k_1 and k_2 :

$$\begin{cases} \sum_{a=1}^{n_a} \sum_{s=1}^{n_s} \frac{\partial(O_{a,s} - Mp_{a,s})^2}{\partial k_1} = 0 \\ \sum_{a=1}^{n_a} \sum_{s=1}^{n_s} \frac{\partial(O_{a,s} - Mp_{a,s})^2}{\partial k_2} = 0 \end{cases} \Leftrightarrow \begin{cases} 2M^2 \sum_{a=1}^{n_a} \sum_{s=1}^{n_s} \left(\frac{\partial p_{a,s}}{\partial k_1} \right)^2 k_1 - 2M \sum_{a=1}^{n_a} \sum_{s=1}^{n_s} \frac{\partial p_{a,s}}{\partial k_1} O_{a,s} = 0 \\ 2M^2 \sum_{a=1}^{n_a} \sum_{s=1}^{n_s} \left(\frac{\partial p_{a,s}}{\partial k_2} \right)^2 k_2 - 2M \sum_{a=1}^{n_a} \sum_{s=1}^{n_s} \frac{\partial p_{a,s}}{\partial k_2} O_{a,s} = 0 \end{cases}$$

$$\Rightarrow \begin{cases} \hat{k}_1 = \frac{\sum_{a=1}^{n_a} \sum_{s=1}^{n_s} O_{a,s} \frac{\partial p_{a,s}}{\partial k_1}}{M \sum_{a=1}^{n_a} \sum_{s=1}^{n_s} \left(\frac{\partial p_{a,s}}{\partial k_1} \right)^2} \\ \hat{k}_2 = \frac{\sum_{a=1}^{n_a} \sum_{s=1}^{n_s} O_{a,s} \frac{\partial p_{a,s}}{\partial k_2}}{M \sum_{a=1}^{n_a} \sum_{s=1}^{n_s} \left(\frac{\partial p_{a,s}}{\partial k_2} \right)^2} \end{cases} \quad (10)$$

where \hat{k}_1 and \hat{k}_2 are estimated coefficient with out the first constraint in Eq. (6), and

$$\frac{\partial p_{a,s}}{\partial k_1} = \frac{2}{3} \left(a^{\frac{3}{2}} - (a-1)^{\frac{3}{2}} \right) \cos \left(\frac{(2s-1)\pi}{n_s} \right) \sin \left(\frac{\pi}{n_s} \right) n_a^{\frac{2}{3}} R^3, \quad (11)$$

$$\frac{\partial p_{a,s}}{\partial k_2} = \frac{2}{3} \left(a^{\frac{3}{2}} - (a-1)^{\frac{3}{2}} \right) \sin \left(\frac{(2s-1)\pi}{n_s} \right) \sin \left(\frac{\pi}{n_s} \right) n_a^{\frac{2}{3}} R^3.$$

Finally we simplify the first constraint in Eq. (6). Notice that f is a linear function, the minimum value $f(\vec{x}_m)$ satisfies

$$\|\vec{x}_m\| = R, \quad (12)$$

and we can further infer that

$$\vec{x}_m = \left(-\frac{k_1}{\sqrt{k_1^2 + k_2^2}} R, -\frac{k_2}{\sqrt{k_1^2 + k_2^2}} R \right). \quad (13)$$

Consequently, the constraint becomes

$$\min f(\vec{x}) = -\sqrt{k_1^2 + k_2^2} R + c \geq 0 \Rightarrow k_1^2 + k_2^2 \leq \frac{1}{\pi^2 R^6}. \quad (14)$$

Notice that the cost function is quadratic related to k_1 and k_2 , we can infer the final value of k_1, k_2 and c as

$$k_1 = \begin{cases} \hat{k}_1, & \text{if } \hat{k}_1^2 + \hat{k}_2^2 \leq \frac{1}{\pi^2 r^6} \\ \frac{\hat{k}_1}{\pi r^3 \sqrt{\hat{k}_1^2 + \hat{k}_2^2}}, & \text{otherwise} \end{cases},$$

$$k_2 = \begin{cases} \hat{k}_2, & \text{if } \hat{k}_1^2 + \hat{k}_2^2 \leq \frac{1}{\pi^2 r^6} \\ \frac{\hat{k}_2}{\pi r^3 \sqrt{\hat{k}_1^2 + \hat{k}_2^2}}, & \text{otherwise} \end{cases}, \quad (15)$$

$$c = \frac{1}{\pi r^2}.$$

6 COMPARISONS OF CPPM WITH DIFFERENT FUNCTIONS

In Section 5, we show that both linear functions and generalized odd functions can be used as sufficient conditions for unbiased estimation. In Table 1, we show the results of APPM, CPPM (using constant functions as described in the main text), CPPM-LF (using linear functions) and CPPM-GOF (using generalized odd functions).

The settings are the same as described in Section 1. CPPM using constant functions performs best. It is true that generalized odd functions have good capability, but a more general hypothetical model is harder to identify the actual distribution accurately. In other words, when the null hypothesis is false, a more general model requires more samples to reject it. Therefore, CPPM-LF and CPPM-GOF do not perform as good as CPPM using linear functions. We demonstrate a typical failure example of CPPM-GOF in Figure 4. But CPPM-GOF has its potential to achieve the best performance after increasing the size of photon map in each pass (a extreme test as shown in Figure 5), which is well corresponding to the underlying theory that GOF covers more general cases.

7 MORE COMPARISONS

We present more comparisons from Figure 6 ~ 14. The settings are identical to that described in Section 1. Our CPPM can always obtain good results. This can demonstrate the ability of CPPM on handling various scenes efficiently.

REFERENCES

- Toshiya Hachisuka and Henrik Wann Jensen. 2009. Stochastic progressive photon mapping. *ACM Transactions on Graphics (TOG)* 28, 5 (2009), 141.
- Henrik Wann Jensen. 2004. A practical guide to global illumination using ray tracing and photon mapping. In *ACM SIGGRAPH 2004 Course Notes*. 20–es.
- Anton S Kaplanyan and Carsten Dachsbacher. 2013. Adaptive progressive photon mapping. *ACM Transactions on Graphics (TOG)* 32, 2 (2013), 16.
- Claude Knous and Matthias Zwicker. 2011. Progressive photon mapping: A probabilistic approach. *ACM Transactions on Graphics (TOG)* 30, 3 (2011), 25.

Table 1. Benchmarks (in alphabetical order) for performance comparison on the iterations and time (sec.) between CPPM and APPM. MSE value obtained from SPPM after 1,000 iterations is used as the baseline. CPPM shows significant improvement over APPM on all scenes and achieve the best performance. CPPM-LF exhibits better performance in most of the benchmarks, while CPPM-GOF shows the worst performance.

Scene		Box	Clocks	Conference	Cornell	Diamond	Dining	Glass	Sibenik	Sponza	Torus	Water
Overview												
MSE \leq		4.825	2.288	12.663	11.494	4.233	19.145	10.525	18.068	15.442	3.500	11.870
SPPM	Iters	1000	1000	1000	1000	1000	1000	1000	1000	1000	1000	1000
	Time	128.685	78.802	108.082	232.403	120.371	166.856	371.223	123.665	70.701	39.254	205.176
APPM	Iters	765	655	538	763	678	961	778	788	823	556	870
	Time	101.415	48.391	62.782	195.307	81.137	162.215	300.411	88.289	56.283	25.091	204.589
CPPM	Iters	376	327	239	547	362	541	582	562	499	252	629
	Time	63.505	24.483	27.614	151.350	59.506	101.389	255.023	69.435	35.861	11.283	176.873
CPPM	-LF	560	404	274	599	577	611	699	821	578	398	815
	Time	88.244	28.96	31.276	162.36	80.834	117.767	326.269	91.447	41.999	17.396	248.606
CPPM	-GOF	698	446	284	640	765	681	795	1084	811	465	1066
	Time	110.713	32.074	32.403	164.516	99.118	127.669	382.189	116.404	56.38	20.232	341.694

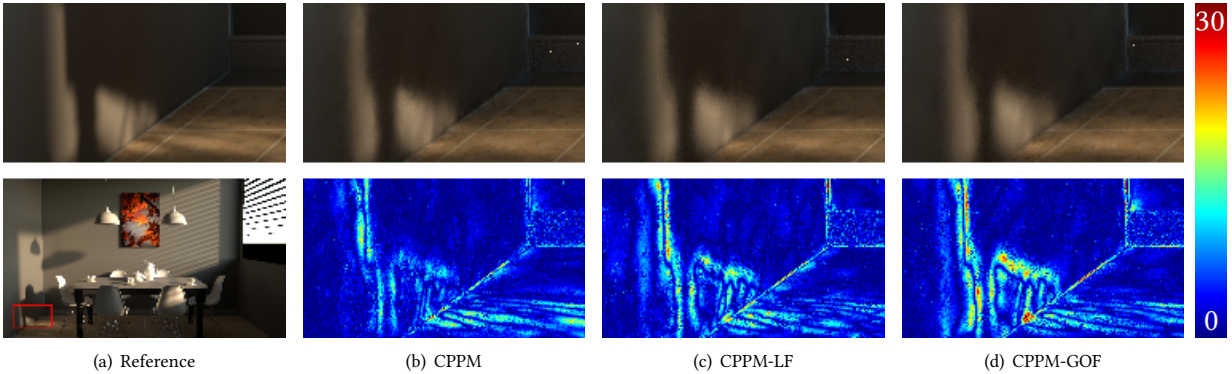


Fig. 4. A typical failure example of CPPM-GOF, while CPPM works well. Close-up images rendered after 1,000 iterations.

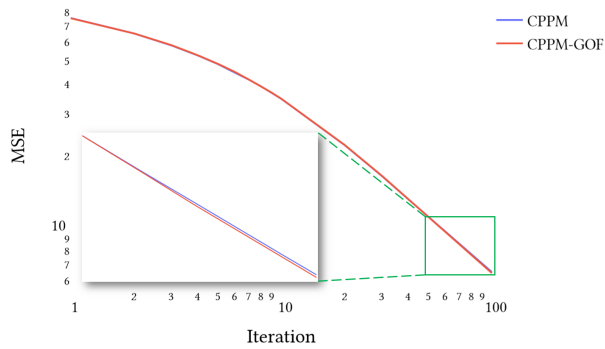


Fig. 5. CPPM and CPPM-GOF on the Box scene using 100×256^2 photons (much more photons than the number of photons used in main text) per iteration.

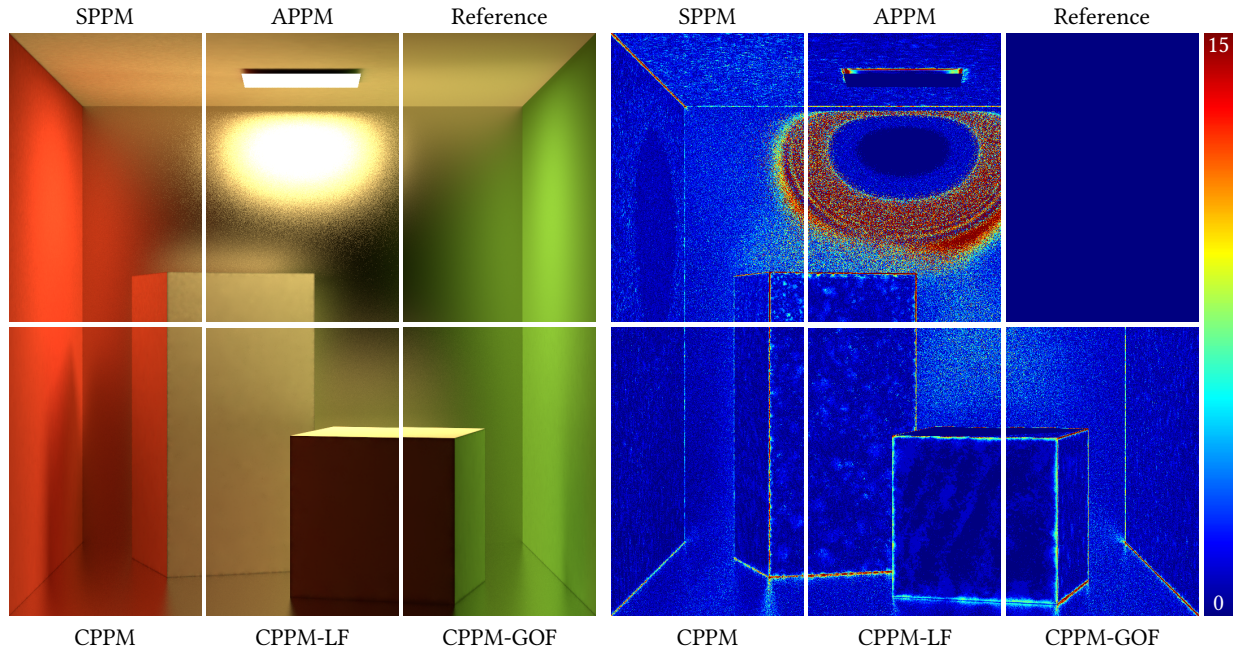


Fig. 6. Comparisons of the Cornell Box scene between different algorithms with 1,000 iterations.

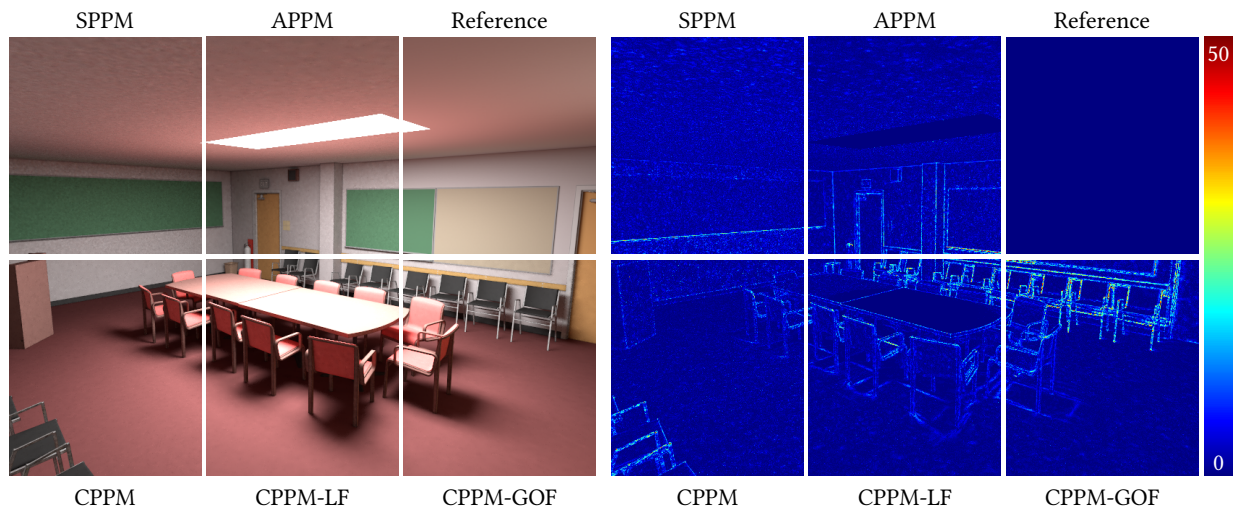


Fig. 7. Comparisons of the Conference scene between different algorithms with 1,000 iterations.

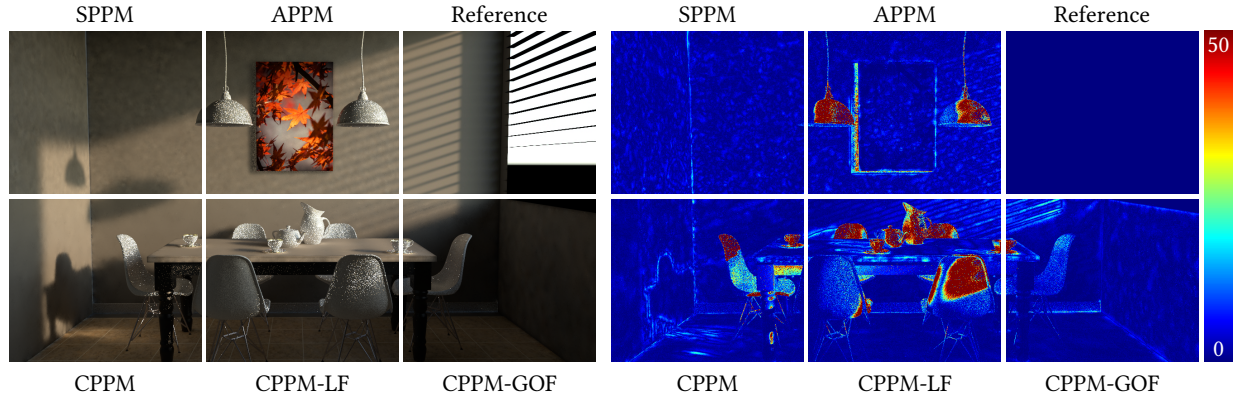


Fig. 8. Comparisons of the Dining scene between different algorithms with 1,000 iterations.

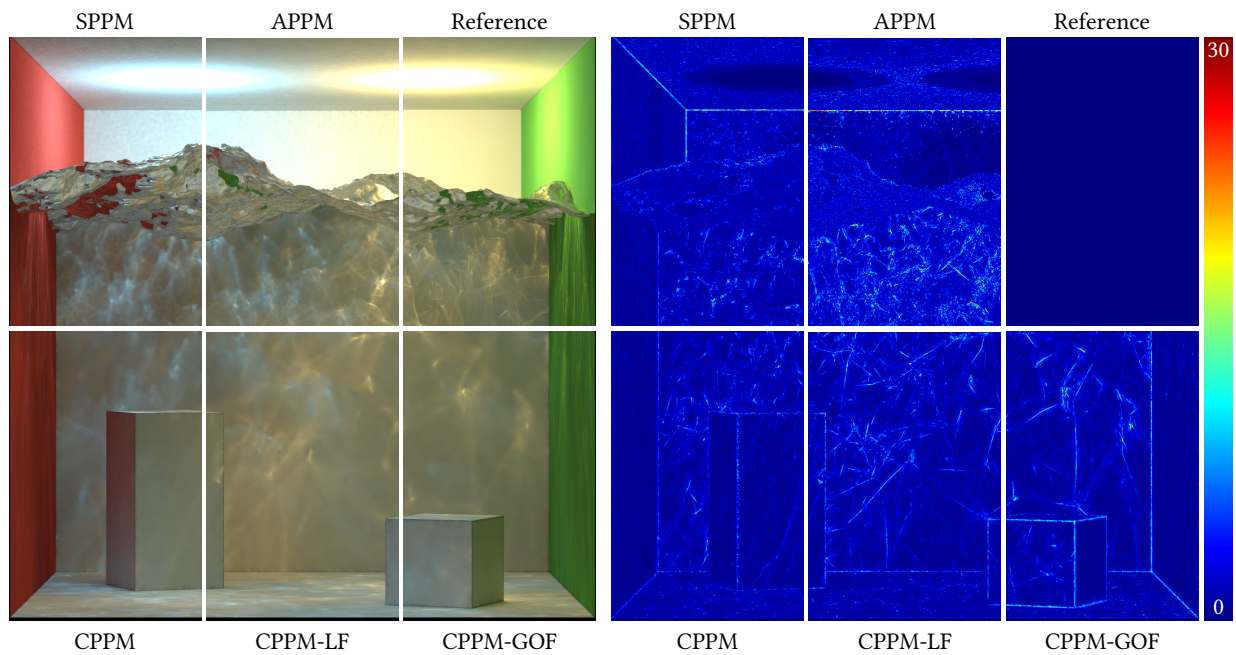


Fig. 9. Comparisons of the Water scene between different algorithms with 1,000 iterations.

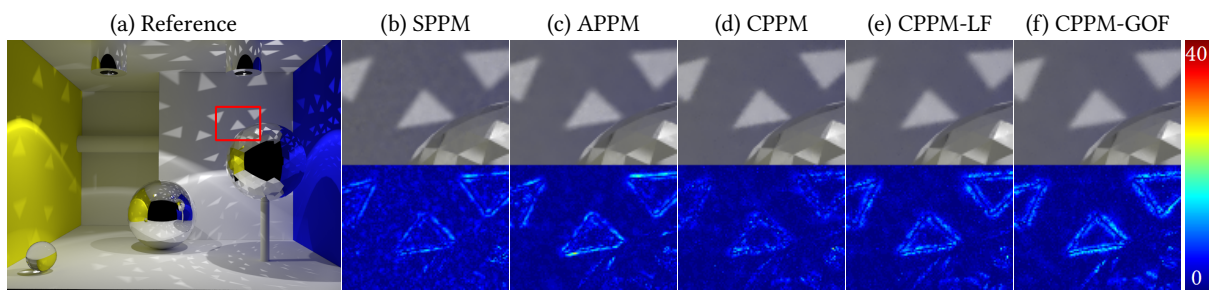


Fig. 10. Close-up images of the Box scene generated by the algorithms with 1,000 iterations. The heat map visualizes the absolute difference w.r.t. the reference image.

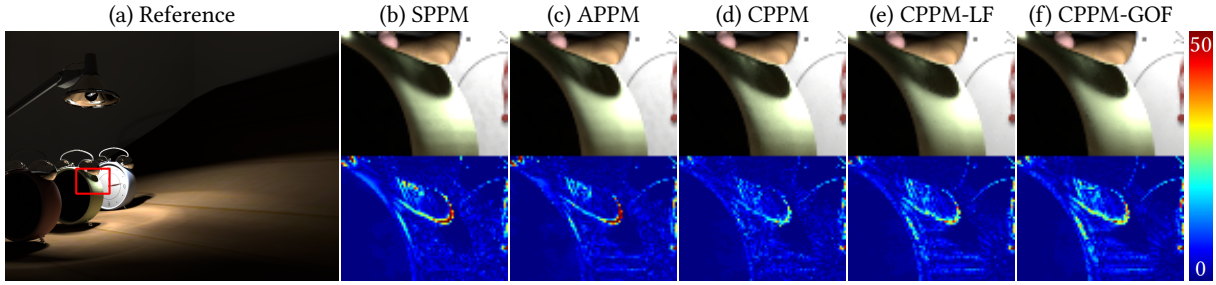


Fig. 11. Close-up images of the Clocks scene generated by different algorithms with 1,000 iterations. The heat map visualizes the absolute difference w.r.t. the reference image.

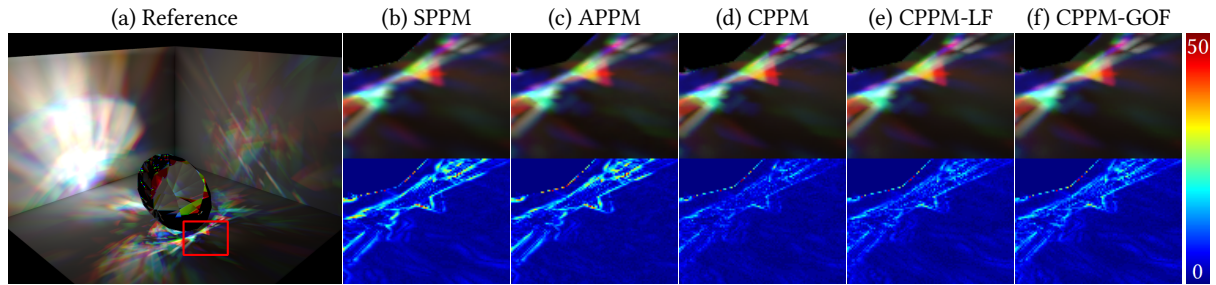


Fig. 12. Close-up images on the Diamond scene generated by different algorithms with 1,000 iterations. The heat map visualizes the absolute difference w.r.t. the reference image.

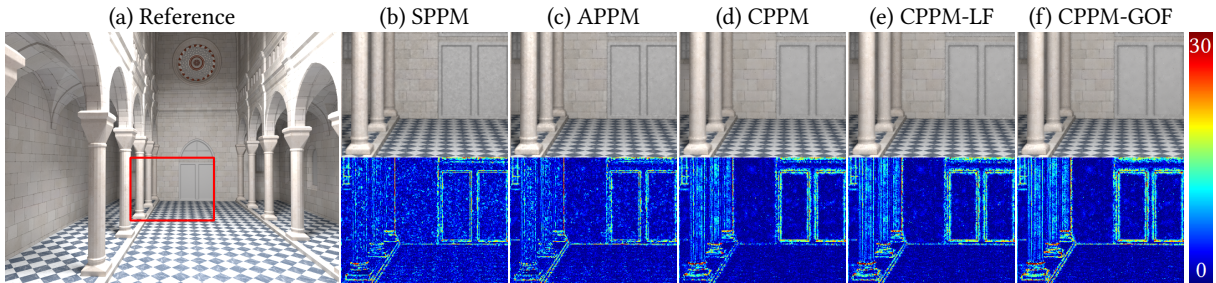


Fig. 13. Close-up images on the Sibenik scene generated by different algorithms with 1,000 iterations. The heat map visualizes the absolute difference w.r.t. the reference image.

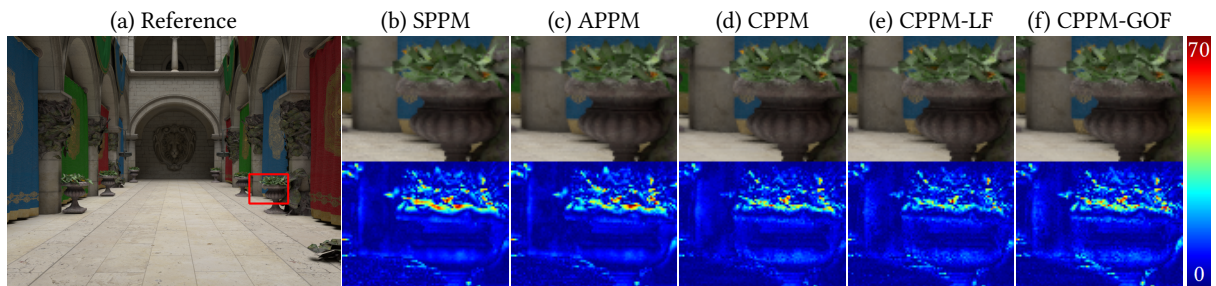


Fig. 14. Close-up images on the Sponza scene generated by different algorithms with 1,000 iterations. The heat map visualizes the absolute difference w.r.t. the reference image.